Analytical Sciences
https://doi.org/10.1007/s44211-022-00209-0

ORIGINAL PAPER

Integration of enzyme-encapsulated mesoporous silica between nanohole array electrode and hydrogel film for flow-type electrochemical biosensor

Daiki Inaba[1] · **Akira Yamaguchi**[1]

Received: 7 September 2022 / Accepted: 27 October 2022
© The Author(s), under exclusive licence to The Japan Society for Analytical Chemistry 2022

Abstract
We herein propose a simple and sensitive electrochemical flow biosensor platform without an external flow device. The sensing unit comprises a platinum nanohole array electrode deposited on a nanoporous track-etched membrane (PtNH/NPM), a packed-layer of glucose oxidase-encapsulated mesoporous silica particles (GOD/MPS), and bovine serum albumin hydrogel film (BSA gel film). This sensing unit was fixed at the open window at the side of the plastic container with internal solution containing NaCl as osmotic reagent. When the sample glucose solution (0.10 mL) was pipetted at the sensing unit, a portion of the sample solution (5 µL) was spontaneously transferred into the BSA gel film. The concentration gradient of NaCl between the internal solution and the BSA gel film induced osmotic flow of water toward the internal solution. This osmotic flow assisted delivery of glucose to the GOD/MPS and enzymatically generated H_2O_2 to the PtNH/NPM. The proposed sensor could be used repeatedly and produced a linear current response for glucose, with a limit of detection of 16 µM. These sensor performances confirmed availability of the sensor design utilizing the osmotic flow.

Keywords Biosensor · Mesoporous silica · Enzyme · Osmotic flow

Introduction

An electrochemical enzymatic biosensor is a conventional tool used for the selective and sensitive detection of biological and environmental substances [1–5]. In the application of the biosensor to monitor a trace biomarker in a biological sample, it is required to enhance activity and stability of an enzyme in the biosensor. Encapsulation of enzyme in a nanoporous host material is one of effective method to meet those requirements [6–11]. For example, it was demonstrated enhanced enzymatic activity and thermal stability of an enzyme encapsulated in various nanoporous host materials [6]. The encapsulated-enzyme can exhibit long-term (60 to 100 days) storage stability [7]. The size matching between pore size and the molecular dimeter of enzyme has been proposed as important factor for the enhanced activity and stability of the encapsulated enzyme [6, 10, 11]. Mesoporous silica materials prepared by supramolecular-templating approach has therefore been used as the host of enzyme due to their uniform pore size of enzyme dimensions [6–11].

The nanoporous host with well-regulated pore structure is usually synthesized as a particulate material. A common method to utilize the particulate nanoporous host for the electrochemical enzymatic biosensor is modification of a detection electrode with the particulate nanoporous host and a supporting matrix [12–19]. On the other hand, several attempts have been made to develop a flow-type biosensor by placing the particulate host materials as 3-dimensional enzyme reactor and a detection electrode separately [20–23]. The separation of biocatalytic and electrode units allows integration of various processes in the biosensor device, resulting in miniaturization of the biosensor device [20, 21]. The miniaturized biosensor has been demanded for home diagnosis and on-site environmental analysis.

The performances of electrochemical flow biosensor are sensitive to the sample injection volume and the bulk solution flow [22]. The sample injection and solution flow are usually controlled by an external pump system, but the pump system increases cost and limits the miniaturization of biosensor device. The pump-free liquid transfer is hence

✉ Akira Yamaguchi
akira.yamaguchi.sci@vc.ibaraki.ac.jp

[1] Institute of Quantum Beam Science, Ibaraki University, 2-1-1 Bunkyo, Mito, Ibaraki 310-8512, Japan

Published online: 05 November 2022

demanded for the development of a small biosensor, and various pump-free fluidic systems that use capillary action [24], hydrostatic pressure [25], osmotic pressure [26–30], and other principles [31] have been studied. Although osmosis is one candidate for active flow in a fluidic channel, its application is currently limited to cell culture [28–30]. An osmosis-driven flow system generally has two reservoirs at both ends of a fluidic channel, with the concentration gradient of the osmotic reagent between two reservoirs inducing the solution flow inside the fluidic channel [31]. The requirement of two reservoirs limits downsizing the sensor device.

We herein propose a simple electrochemical flow biosensor platform that integrates multiple functions, such as sample injection, transport of a target analyte, enzymatic reaction, signal transduction. The performance of the proposed sensor device was examined by electrochemical detection of H_2O_2 produced by enzymatic glucose oxidation. A schematic diagram of our proposed sensor is shown in Fig. 1 (A) and (B). The glucose sensing unit comprises bovine serum albumin hydrogel film (BSA gel film), a packed-bed type enzyme reactor based on glucose oxidase-immobilized mesoporous silica powders (GOD/MPS), and a platinum nanohole array electrode on a nanoporous Track-etched membrane (PtNH/NPM). This sensing unit is attached to the open window at the side of the plastic container with NaCl aqueous solution (internal solution). A hydrophobic polyethylene terephthalate (PET) film with an open window was used to fix the BSA gel film.

The BSA gel film can be easily prepared by heating a BSA solution [32, 33], and it plays main role in the capture of sample glucose solution and the pump-free transport of glucose in the sensing unit. The BSA gel film is initially made to shrink because it is connected to the high ionic strength solution in the plastic container (Fig. S1). When a sample glucose solution containing no NaCl is pipetted on the upper side of the sensing unit (Fig. 1A), the sample solution immediately falls along the sensor wall by gravity (Fig. S2). During the descent of the sample droplet, a portion of sample solution was captured at the BSA gel film surrounded by the hydrophobic PET film. Then, the BSA gel film absorbs the captured solution (Fig. 1 (C)). The sample solution is thus spontaneously introduced into the sensing unit. The NaCl concentration in the sample solution captured at the BSA gel is initially lower than that of the internal solution. This concentration gradient of NaCl (osmotic reagent) induces osmotic flow of water toward the internal solution (Fig. 1 (C)). NaCl is used as supporting electrolyte for the electrochemical measurement and the osmotic reagent. The BSA gel film acts as a pseudo inlet reservoir. We thus anticipated that the osmotic flow could deliver glucose captured at the BSA gel film to the enzyme reactor and detection electrode positioned downstream of the BSA gel film. The BSA gel is a kind of hydrogel, and hydrophilic molecules

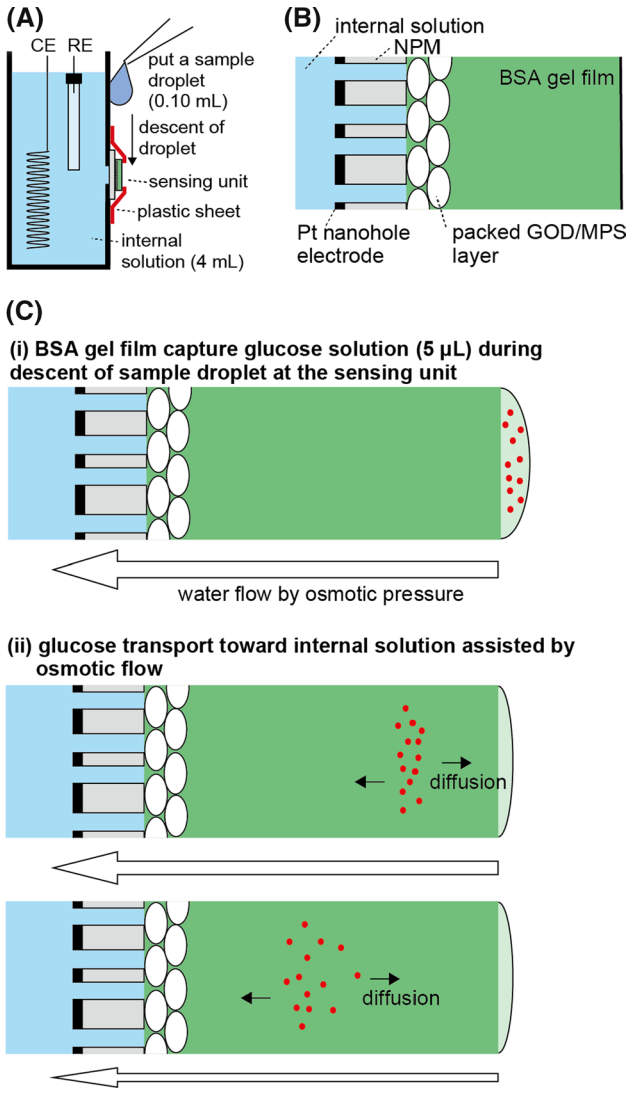

Fig. 1 Schematic diagram of **A** sensor device and **B** sensing unit. **C** Scheme of pump-free transport of glucose toward the internal solution assisted by osmotic flow of water

and ions can move freely in its film. We considered that the BSA gel was suitable for transport of hydrophilic glucose and H_2O_2 assisted by the osmotic flow.

The packed-bed type enzyme reactor is one of candidate for the efficient glucose/H_2O_2 conversion in a fluidic system, because glucose always passes through the three-dimensional enzyme reactor [20, 22]. The Pt nanohole array electrode is also suitable nanoscale electrode for efficient electrochemical oxidation of H_2O_2 due to high collision frequency of H_2O_2 with the Pt nanohole [22]. We thus integrated the packed layer of GOD/MPS between the BSA gel film and the PtNH/NPM. The unreacted glucose and H_2O_2 are diluted into the large-volume solution in the plastic container by the osmotic flow and self-diffusion, so that those spontaneously leave away from the detection electrode.

On the basis of the above schematic diagram, we fabricated the glucose sensor device. In the present study, the pump-free transport of an analyte by the osmotic flow was examined at first, after which the sensor performance for glucose detection was examined.

Experimental

Materials and chemicals

Pluronic® P-123 (P123), bovine serum albumin (BSA), and glucose oxidase (GOD) were purchased from Sigma-Aldrich Japan (Tokyo, Japan). 3-Aminopropyltriethoxysilane (APTES) and potassium hexacyanoferrate (II) were purchased from Kishida Chemical Co., Ltd. (Osaka, Japan). Glucose was purchased from Tokyo Chemical Industry Co., Ltd. (Tokyo, Japan). Tetraethoxysilane (TEOS), dry tetrahydrofuran (THF) and all other chemicals were purchased from Fujifilm Wako Pure Chemical Corp. (Osaka, Japan). Cyclopore™ track etched (TE) membrane (thickness = 15 µm, pore size = 200 nm, and porosity = 15%) and Anodisc porous alumina (PA) membrane (thickness = 60 µm, pore size = 200 nm, and porosity = 40%) were purchased from Whatman International Ltd. (England). Milli-Q water was used in all the experiments.

Preparation of BSA gel film

BSA gel film was synthesized by heat denaturation of BSA [33]. The isoelectric point of BSA is at pH 4.5–5.0. The BSA solution (15 wt%) was poured into a home-made plastic mold (diameter = 8 mm, depth = 0.5 mm), and the mold was held at 80 °C for 30 min. Figure 1 (A) shows typical photo of the BSA gel film.

Synthesis of GOD/MPS

Particulate mesoporous silica was synthesized according to the literature [34] with some modifications. A mixture of P123 (1.3 g), 2 M hydrochloric acid (40 g), and water (10 g) was stirred at 40 °C for 2 h. TEOS (3.0 g) was then added to the mixture and the mixed solution was stirred for at 40 °C for 24 h. The mixture was then sealed in an autoclave and held at 150 ˚C for 48 h. The solid product was filtered, washed with water, and dried at 101 °C for 8 h. The final product was calcined at 540 °C for 48 h to remove the template surfactant. Figure 2 (B) shows a typical field-emission scanning electron microscopy (FE-SEM, Hitachi S4800) image of the mesoporous silica. The surface of mesoporous silica was modified with APTES [35]. The pore structures of the mesoporous silicas were characterized by small-angle X-ray scattering (SAXS, Rigaku Smartlab), and nitrogen adsorption/desorption isotherm (Micrometrics ASAP 2020). The pore distribution plots and SAXS profiled are shown in Fig. S3. The structural parameters of the mesoporous silicas are summarized in Table S1. The BET surface area, pore volume, and pore diameter decreased after the APTES modification, indicating formation of aminopropyl-layer at the inner pore wall of mesoporous silica.

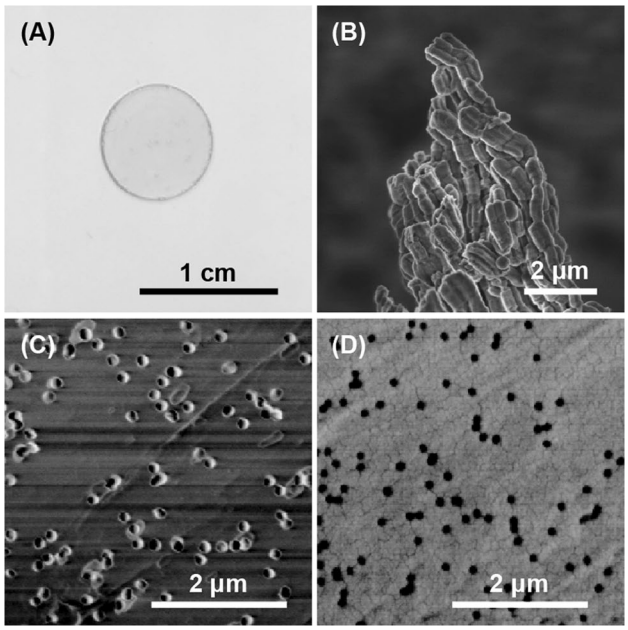

Fig. 2 **A** Photo of BSA gel film, **B** SEM image of mesoporous silica, and nanoporous track-etched membranes **C** before and **D** after Pt deposition

The aminopropyl-modified mesoporous silica (3 mg) was added to 1 mL of 100 mM phosphate buffer solution (pH 5) containing 1 mg GOD. After being shaken for 20 h at 22 °C, the mixture was centrifuged at 12,000 rpm for 10 min. The supernatant was subjected to adsorption spectrum measurement to estimate the amount of GOD encapsulated. The resulting aminopropyl-modified mesoporous silica with GOD (GOD/MPS) was carefully rinsed with the buffer solution. The amount of GOD adsorbed at pH 5 was 0.146 g g^{-1} (Fig. S4). This value suggests 24% of the pore volume to be occupied by GOD molecules, that is, the GOD molecules were densely encapsulated within the amine-functionalized mesoporous silica.

Fabrication of PtNH/NPM

A Pt layer was deposited on the nanoporous membrane (TE or PA membrane) by sputter deposition using an ion-sputtering system (Hitachi, Model E-1045). Figure 2 (C) and (D) show SEM images of TE membrane before/after the Pt deposition. The pore structure of the TE membrane was maintained after the Pt deposition. The Pt layer deposited

on the TE surface could be used as a working electrode, as shown in cyclic voltammogram of potassium ferricyanide (Fig. S5). SEM images of PA membranes are shown in Fig. S6. The Pt deposition on the PA narrowed the pore entrance because of small inter-pore distance. The Pt-deposited PA membrane was used to examine the reproducibility of the amperometric glucose sensing.

Sensor fabrication and electrochemical measurement

The sensor scheme is shown in Fig. 1 (A) and (B). First, the PtNH/NPM was glued over the open window (4 mm in diameter) of a square plastic container. After locating the packed layer of GOD/MPS on the Pt/NPM, the BSA gel film was pressed onto the packed GOD/MPS layer. Finally, a hydrophobic polyethylene terephthalate (PET) film (0.1 mm in thickness) with an open window (6 mm in diameter) was glued to fix the BSA gel. The internal solution in the plastic container was 3 M or 5 M NaCl aqueous solution containing 50 mM phosphate buffer (pH 7). Pt wire and Ag/AgCl reference electrodes were immersed in the internal solution for electrochemical measurements. Electrochemical measurement was performed using an electrochemical analyzer (CH Instruments, Inc., ALS/chi Model 701A). Glucose sample solution (0.10 mL) was dropped on the upper side of the BSA gel film by hand pipetting (Fig. 1 (A)). The sample solution immediately descended along the sensor wall (Fig. S2). The electrochemical reaction that took place at the Pt nanohole array electrode was monitored by chronoamperometry at a potential of 0.6 V vs. Ag/AgCl. The oxidation current of $Fe(CN)_6^{4-}$ or H_2O_2 was corrected by subtracting the base current.

Results and discussion

Evaluation of the osmotic flow in the sensing unit

In the study on the pump-free transport behavior of an analyte, we fabricated a simple sensing unit by attaching the BSA gel film on the PtNH/NPM (inset of Fig. 3 (A)). The resulting device was used to examine the electrochemical responses upon application of a droplet of 1 mM $K_4Fe(CN)_6$ solution. Asymmetric current peak was observed upon pipetting of the sample droplet (Fig. 3 (A)). When the sample droplet was pipetted during a continuous cyclic voltammetry (CV) cycling, redox peaks of $Fe(CN)_6^{4-}$ appeared after the pipetting of the $K_4Fe(CN)_6$ solution (Fig. S7). The redox peaks increased once with the potential cycle and then decreased. The asymmetric current peak was hence ascribed to oxidation of $Fe(CN)_6^{4-}$, which was captured during the descent of the sample droplet at the sensing unit.

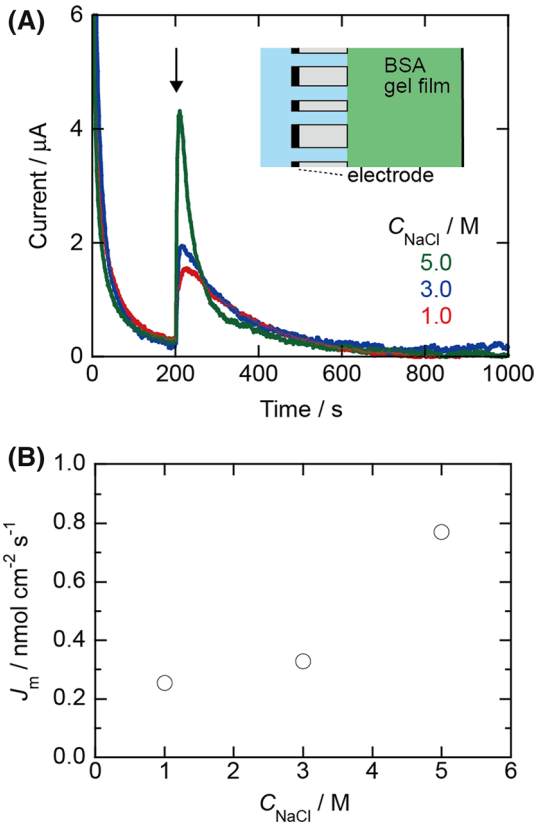

Fig. 3 **A** Amperometric responses upon pipetting of droplet containing 1.0 mM $K_4Fe(CN)_6$. Arrow indicates time of the pipetting. Inset shows schematic diagram of the simple sensing unit used for the evaluation of the osmotic flow. **B** Relationship between initial mass transport flux of $Fe(CN)_6^{4-}$ (J_m) and concentration of NaCl in the internal solution (C_{NaCl})

The volume of water captured at the BSA gel film was determined by measuring weight loss of water droplet (0.10 mL) after descent at the sensing unit. The capture volume for ten individual measurements was 5.0 to 5.1 μL (Table 1) and was independent of the concentration of NaCl in the internal solution (C_{NaCl}). In the sensing unit, the BSA gel film was fixed by the hydrophobic PET film (0.1 mm in thickness) with open window (6 mm in diameter). The initial thickness of the sample solution captured at the BSA gel film (5 μL) was hence calculated to be 1.8 times larger than the thickness of the PET film (Fig. S2). It is hence considered that the capture volume is determined in part by the surface tension at the hydrophobic boundary of the PET film.

Although the volume of water solution captured at the BSA gel film was independent of C_{NaCl}, the oxidation current peak became larger with increasing C_{NaCl}. In addition, the time for appearance of peak maximum (peak time) tended to be shorter with increasing C_{NaCl}. The parameters of the current peaks are summarized in Table 1.

Table 1 Parameters of current peaks in Fig. 3 (A), volume of water captured at BSA gel film, and overall electrochemical conversion yield

	C_{NaCl} / M		
	1	3	5
Peak intensity / μA	1.3	1.7	4.0
Peak time[a]/s	27 (30)[e]	17 (24)[e]	11 (10)[e]
Peak width[b]/s	120	102	39
Peak area/μC	196	210	213
Conversion[c]/%	41	44	43
V_c[d]/μL	5.1 ± 1.1	5.0 ± 1.2	5.0 ± 1.1

[a]Time for maximum current

[b]Width at half of peak height

[c]Overall electrochemical conversion yield of $Fe(CN)_6^{4-}$

[d]Volume of water captured at the BSA gel film ($n = 10$)

[e]Peak time calculated by the initial flux of $Fe(CN)_6^{4-}$

We estimated the initial mass transport flux (J_m) of $Fe(CN)_6^{4-}$ across the PtNH/NPM. This estimation is based on general form for a mass transport flux across a porous membrane [36]. On the assumption that the peak intensity of the oxidation current reflects the initial mass transport flux, J_m is described by Eq. (1).

$$J_m = \frac{Q}{F\phi} \times \frac{1}{2\pi R_m^2 \theta} \quad (1)$$

Q is amount of electric charge per second at the peak maximum, and F is Faraday constant. R_m is radius of the PtNH/NPM exposed to the internal solution (2 mm). θ is porosity of the TE membrane (15%). f is conversion efficiency of $Fe(CN)_6^{4-}$ to the oxidation current. Herein, the overall electrochemical conversion yield of $Fe(CN)_6^{4-}$ was calculated by $A_{peak}V_c/(F \times C_{Fe})$, where A_{peak} is peak area shown in Fig. 3 (A), F is Faraday constant. C_{Fe} is concentration of $Fe(CN)_6^{4-}$, and V_c is volume of water captured at the BSA gel film (Table 1). The estimated overall conversion yield (Table 1) was used as f. As shown in Fig. 3 (B), the estimated J_m was almost proportional to C_{NaCl}. This quasi-linear relationship indicates that the transport of $Fe(CN)_6^{4-}$ toward the internal solution is facilitated by the osmotic flow of water, because the osmotic pressure across a membrane is proportional to concentration difference of an osmotic reagent between two solution phases [27].

The linear velocities of $Fe(CN)_6^{4-}$ was calculated by assuming that the initial flux of $Fe(CN)_6^{4-}$ is due to the steady flow of 1 mM $K_4Fe(CN)_6$ solution in the sensing unit. The estimated linear velocities were 17 μm s^{-1} for $C_{NaCl} = 1$ M, 22 μm s^{-1} for $C_{NaCl} = 3$ M, and 51 μm s^{-1} for $C_{NaCl} = 5$ M. When these linear velocities were used to calculate the time to transport of $Fe(CN)_6^{4-}$ across the BSA gel film (500 μm) and PtNH/NPM (15 μm), the calculated times were consistent with the peak times (Table 1). This consistency confirms that the transport of $Fe(CN)_6^{4-}$ toward the internal solution is assisted by the osmotic flow of water.

In simple membrane diffusion model, the initial flux of $Fe(CN)_6^{4-}$ across the BSA gel film (J_{diff}) is described by $J_{diff} = D\Delta C/l$ [36]. l is thickness of the BSA gel film. ΔC is initial concentration difference of $Fe(CN)_6^{4-}$ between the solution captured at the BSA gel film and the internal solution. D is diffusion coefficient of $Fe(CN)_6^{4-}$ in the BSA gel film. Herein, D was estimated from that in a bulk water by Ogston model (1.5×10^{-6} cm^2 s^{-1} in 15 wt% BSA gel film) [37, 38]. The calculated J_{diff} was 3.1×10^{-12} mol cm^{-2} s^{-1}, which was two orders of magnitude smaller than J_m (Fig. 3 (B)), indicating less contribution of the diffusion process to the initial transport of $Fe(CN)_6^{4-}$ toward the internal solution. On the other hand, the osmotic pressure by the concentration gradient of NaCl should decrease with time, because the volume of BSA gel film and the captured solution are much smaller than that of the internal solution. It is hence considered that contribution of the diffusion process to the overall transport behavior of $Fe(CN)_6^{4-}$ becomes larger after time has passed. The forward and back diffusion of $Fe(CN)_6^{4-}$ causes the spreading and tailing of the current peak as schematically shown in Fig. 1 (C).

The results on the transport of $Fe(CN)_6^{4-}$ in the simple sensing unit are follows: (i) 5 μL of sample solution is spontaneously captured at the sensing unit, (ii) transport of $Fe(CN)_6^{4-}$ toward the internal solution is assisted by osmotic flow of water, and higher osmotic flow produces greater oxidation current peak, (iii) the diffusion of $Fe(CN)_6^{4-}$ is related to the width of the oxidation current peak.

Amperometric response for glucose solution

Figure 4 (A) and (B) shows typical amperometric profiles obtained for the sensor device comprising of PtNH/NPM, GOD/MPS, and BSA gel film. When a droplet of pure water was pipetted at the sensing unit, a fast amperometric spike was observed (Fig. 4 (A)). This fast spike is ascribed to non-Faradic current. The osmotic flow of water perturbs the distribution of electrolytes in the vicinity of the Pt nanohole electrode, and this perturbation of the electrolyte manifests as a fast amperometric spike. In contrast, a broad and asymmetric current peak was observed upon pipetting of the glucose solution. The amplitude of this broad peak became greater on increasing the glucose concentration in the droplet (Fig. 4 (A) and (B)). These results indicate that the broad peak is due to electrochemical oxidation of H_2O_2, which is by-product of glucose oxidation at the packed-layer of GOD/MPS.

The reproducibility of the amperometric response was examined for pipetting of 0.1 mM and1.0 mM glucose

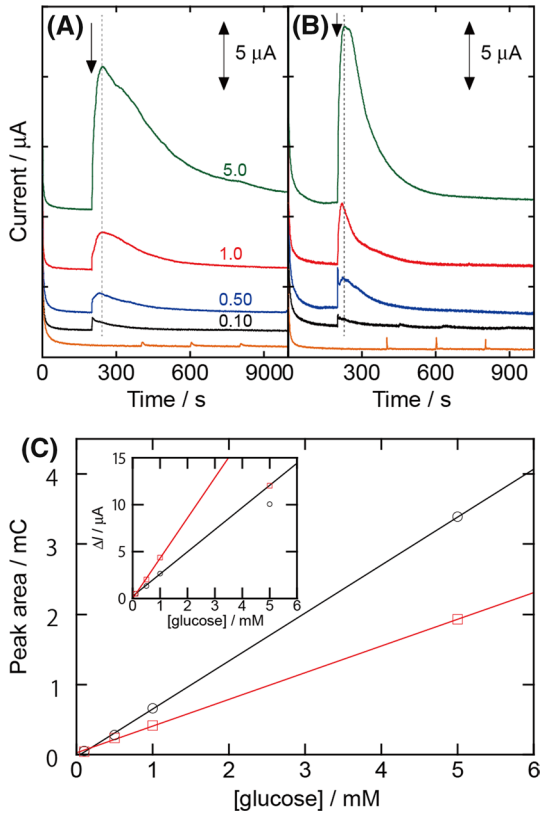

Fig. 4 Amperometric responses upon pipetting of glucose solution (0.10 mL). NaCl concentrations in the internal solution (C_{NaCl}) are **A** 3.0 M and **B** 5.0 M. The bottom orange lines in **A** and **B** are amperometric responses upon pipetting of pure water. The arrow indicates the time at which the pipetting of sample solution. Relationships between the peak area and the glucose concentration for C_{NaCl} = 3.0 M (black open circles) and C_{NaCl} = 5.0 M (red open squares). The solid lines show linear regression of data (glucose concentration: 0.10–5.0 mM). Inset shows relationships between the current response (ΔI) and the glucose concentration for C_{NaCl} = 3.0 M (black open circles) and C_{NaCl} = 5.0 M (red open squares). The current response was obtained at 40 s (C_{NaCl} = 3.0 M) or 20 s (C_{NaCl} = 5.0 M) after the pipetting of sample solutions (represented by gray dashed-line in (A) and (B)). The solid lines show linear regression of data (glucose concentration: 0.10–1.0 mM)

solution. As shown in Fig. S8, repeatable amperometric response was observed for three or four time measurements. For the pipetting of 1.0 mM glucose solution, the relative standard deviations (RSD) of peak area and peak intensity were 5.7 and 6.8%, respectively. RSD values for the pipetting of 0.1 mM glucose solution were 7.2% for peak area and 15% for peak intensity.

As shown in Fig. 4 (A) and (B), the fast spike due to the non-Faradic current appeared in the amperometric response upon pipetting of low concentration glucose solution. The comparison of the current spike and the oxidation current observed for the pipetting of 0.10 mM glucose solution is shown in Fig. S9. In the sensor with 3 M of C_{NaCl}, the non-Faradic current decayed to less than 3.3σ after 40 s from the application of the glucose solution (Fig. S9 (A)). σ is the standard deviation of the background current. The peak times for the application of the glucose solutions ranging from 0.5 to 5.0 mM were around 40 s (see gray dashed-line in Fig. 4 (A)). In the sensor with 5 M of C_{NaCl}, the peak times were around 20 s (see gray dashed line in Fig. 4 (B)). The non-Faradic current decayed to less than 3σ after 20 s from the application of the glucose solution (Fig. S9 (B)). Herein, we hence defined the current response toward the glucose as $\Delta I = I_x - I_0$, where I_0 is current value just before the sample application. I_x is the current value after x seconds from the sample application; x was 40 s (3 M of C_{NaCl}) or 20 s (5 M of C_{NaCl}). I_x corresponds to the peak current intensity for the pipetting of high-concentration glucose solution.

The area of the current spikes were 5.0 ± 1.2 μC for 3 M of C_{NaCl} and 4.4 ± 2.0 μC for 5 M of C_{NaCl}. These peak areas were one order of magnitude smaller than those for the application of 0.1 mM glucose solution (53μC for 3 M of C_{NaCl} and 41 μC for 5 M of C_{NaCl}). The overall current change upon pipetting of the glucose solution was therefore used to estimate the peak area of the oxidation current.

The peak area of the oxidation current provided information on the overall conversion, involving glucose/H_2O_2 conversion at GOD/MPS and H_2O_2/signal conversion at the PtNH. As shown in Fig. 4 (C), linear relationships between the peak area and the glucose concentration were obtained over the concentration range of 0.1–5.0 mM with a correlation coefficient of 0.999. With the sample volume captured at the BSA gel film was 5 μL (Table 1), we estimated the overall conversion yield of glucose from the slope of correlation. The estimated yields were 66% for 3 M of C_{NaCl} and 43% for 5 M. The overall conversion yield tended to decrease on increasing C_{NaCl}. This tendency was observed for sensor devices with different nanoporous membrane (Fig. S10). It was therefore concluded that deterioration of the GOD activity in higher ionic strength condition results in decreasing the enzymatic conversion of glucose at the packed-layer of GOD/MPS [39].

The loss of overall enzymatic activity of GOD is related to conformational change, bimolecular rate constant between GOD and substrates, and mass transport behaviors of substrates on the GOD/MPS. Ahmad et al. studied conformation, stability, and activity of GOD in NaCl concentration range of 0.02 and 2 M [40]. They found that the enzymatic activity of GOD was not influenced by the NaCl concentration. The addition of large amount of NaCl (2 M) stabilized GOD against thermal denaturation and slightly enhanced the affinity of glucose for GOD. Sugimoto et al. reported that the bimolecular rate constant for glucose oxidation at GOD with uncharged redox mediator (quinone) was independent on the ionic strength over the range of 0.01–0.25 M [41]. Results on these ionic strength dependencies for bulk solution systems suggest that the GOD activity is insensitive to the NaCl

concentration. On the other hand, interfacial mass transfer of substances (glucose and H_2O_2) at the mesoporous silica pores will become slower on increasing the NaCl concentration, because the solution viscosity increases with increasing NaCl concentration [42]. The viscosity of 5 M NaCl solution is about 1.2 times higher than that of 3 M NaCl solution [42]. We hence consider that the slow mass transfer process at GOD/MPS in viscous medium is due to the apparent deterioration of the GOD activity for 5 M of C_{NaCl}.

In spite of the lower GOD activity, more intense current peak was observed for C_{NaCl} = 5 M (inset of Fig. 4(C)), owing to the faster osmotic flow. The linear relationships between glucose concentration and current response were obtained over the range of 0.1–1.0 mM with a correlation coefficient of 0.998, while obvious deviation from the linear relationship was observed for high glucose concentration (5.0 mM). Contribution of the diffusion-based flux of glucose (J_{diff}) to the overall transport behavior of an analyte increases with increasing the glucose concentration. This diffusion-based flux would induce spreading of the glucose distribution as schematically shown in Fig. 1 (C), resulting in decrease in the peak intensity.

In the amperometric sensing, improvement of current peak intensity is most important for the sensitive detection. We hence examined the detailed sensor response for the device with the internal solution containing 5 M of NaCl.

Sensor response for successive sample pipetting

Figure 5 (A) shows amperometric profiles observed upon successive pipetting of a sample droplet containing glucose ranging from 0.010 to 5.0 mM, together with amperometric profiles for the pipetting of pure water. Since the upper limit of the measurement time was 1000 s for the electrochemical analyzer used in this study, the amperometric profile depended on the glucose concentration was obtained in three measurements. The current sensor response upon pipetting of the glucose solution was defined as $\Delta I = I_{20} - I_0$ as discussed before. As shown in Fig. 5 (B), the sensor response showed linear relationship with the glucose concentration over the range of 0.01–1.0 mM (correlation coefficient: 0.997). Deviation from the linear relationship was observed for the application of high glucose concentration (5.0 mM). The limit of detection, defined as LOD = $3.3\sigma/S$, where σ is the standard deviation of the blank (0.017 µA) and S is the slope of the calibration curve (3.5 µA mM^{-1}), was 0.016 mM. The sensor sensitivity was 28 µA cm^{-2} mM^{-1}. These sensor performances indicate availability of the present sensor platform for a flow-injection analysis (FIA) type electrochemical biosensor.

When the glucose concentration was less than 0.1 mM, the interference of the fast spike due to the non-Faradic current on the glucose sensing was significant (Fig. 5 (A)).

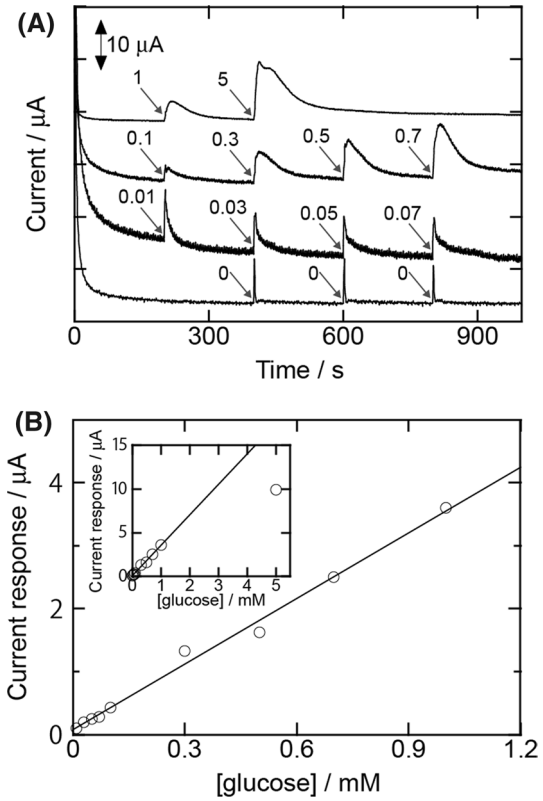

Fig. 5 **A** Amperometric responses for successive pipetting of glucose solution (0.010 to 5.0 mM). C_{NaCl} is 5.0 M. **B** Relationship between the current response and the glucose concentration. The current response was obtained at 20 s after the pipetting of sample solution. The solid lines show linear regression of data (glucose concentration: 0.10–1.0 mM). Inset shows the sensor response including data for the pipettng of 5.0 mM glucose solution

However, it could be reduced or eliminated by choosing the appropriate time (20 s for 5 M of C_{NaCl}) after the sample pipetting. As shown in Fig. 5 (A), the oxidative current did not decay to background level after 200 s from the sample pipetting. In the pipetting of 0.1–1.0 mM glucose solution, the oxidation current decayed to about 8% of the maximum value (peak current intensity). This result indicates that a small portion of glucose and/or H_2O_2 are remained in the sensing unit. Since the linear sensor response could be obtained, the remained substances did not significantly affect the sensor response for the successive pipetting of the glucose solution.

In a FIA-type electrochemical enzymatic sensor, the enzymatic conversion and electrochemical signal transduction processes depend on the sample injection volume and the bulk solution flow [22]. An external flow device to regulate those factors is hence connected to the sensing unit. The FIA-type electrochemical glucose sensors with a packed-bed type enzyme reactor and an external flow device showed LOD of 0.011 to 0.06 mM [20, 22], which are comparable to

that of the present sensor. It can therefore be concluded that transport of glucose and H_2O_2 assisted by the osmotic flow is useful for simple and sensitive pump-free flow sensing.

Glucose concentrations in healthy patients are 0.06–0.11 mM in sweat, 0.23–0.38 mM in saliva, and 0.05–0.5 mM in ocular fluid [43]. The LOD of the present sensors is in the range of glucose concentrations from those non-invasive samples. On the other hand, the glucose concentration in a blood (ca. 5 mM) exceeds the linear range of the present sensor. The present sensor has potential for glucose sensing of invasive samples rather than a blood sample. Since the present sensor response is oxidation current of H_2O_2 at a potential of 0.6 V vs. Ag/AgCl, various redox-active substances such as dopamine and ascorbate will interferer the detection of glucose [44]. It is expected that the sensing unit without GOD/MPS provides no oxidation current of H_2O_2, which is by-product of glucose oxidation at the packed-layer of GOD/MPS. The integration of the sensing units with/without GOD/MPS will eliminate the interference from the redox-active substances.

The results on the simple sensing unit indicated that the peak current was mainly governed by the velocities of a redox-active species in the BSA gel film and the nanochannels in the nanoporous membrane. The velocity depends on the osmotic flow rate, thickness and density of BSA gel thickness, inter-molecular interaction in the BSA gel film and in the nanochannels, and porosity and thickness of the nanoporous membrane. Optimization of these factors will improve the peak current and the sensor sensitivity.

Conclusion

IN this study, we fabricated the flow-type electrochemical biosensor by integrating the packed layer of GOD/MPS as the enzyme reactor between the BSA gel film and the PtNH/NPM. The sensor could spontaneously capture a small portion (5 µL) of sample glucose solution, which was handpipetted at the sensor device. The osmotic flow induced by concentration gradient of NaCl (osmotic reagent) assisted transport of the captured glucose to the GOD/MPS and H_2O_2 to the Pt nanohole array electrode. The present sensor could thus work as flow-type sensor without an external flow device.

The increase in the concentration gradient of NaCl facilitated the transport of glucose and H_2O_2. The facilitated transport behaviors improved the current sensor response in spite of the loss of GOD activity. The current sensor response was interfered from non-Faradic current due to perturbation of electrolyte distribution in the vicinity of the Pt nanohole electrode, but the interference could be eliminated by choosing the appropriate measurement time. After optimization of the detection conditions, the sensor showed linear responses in the range from 0.01 to 1.0 mM for glucose with LOD of 16 µM. The RSD of amperometric responses found for the application of 1 mM glucose solution was 6%. These sensor performances indicate availability of the present sensor design utilizing the osmotic flow for simple and sensitive electrochemical flow biosensor.

Supplementary Information The online version contains supplementary material available at https://doi.org/10.1007/s44211-022-00209-0.

Acknowledgements This work was supported in part by JSPS KAKENHI Grant Numbers 16H04160 and 22K05168, and Takahashi Industrial and Economic Research Foundation.

Data Availability All data generated or analysed during this study are included in this published article and its supplementary information file.

Declarations

Conflict of interest There are no conflicts to declare.

References

1. D.W. Kimmel, G. LeBlanc, M.E. Meschievitz, D.E. Cliffel, Anal. Chem. **84**, 685 (2012)
2. C. Chen, Q. Xie, D. Yang, H. Xiao, Y. Fu, Y. Tan, S. Yao, RSC Adv. **3**, 4473 (2013)
3. K. Mathwig, T. Albrecht, E.D. Goluch, L. Rassaei, Anal. Chem. **87**, 5470 (2015)
4. C. Zhu, G. Yang, H. Li, D. Du, Y. Lin, Anal. Chem. **87**, 230 (2015)
5. H. Lee, Y.J. Hong, S. Baik, T. Hyeon, D.-H. Kim, Adv. Healthc. Mater. **7**, 1701150 (2018)
6. K.-C. Kao, T.-S. Lin, C.-Y. Mou, J. Phys. Chem. C **118**, 6734 (2014)
7. T. Shimomura, T. Itoh, T. Sumiya, F. Mizukami, M. Ono, Sens. Actuators B **135**, 268 (2008)
8. A. Küchler, M. Yoshimoto, S. Luginbühl, F. Mavelli, P. Walde, Nat. Nanotechnol. **11**, 409 (2016)
9. A. Walcarius, Curr. Opin. Electrochem. **10**, 88 (2018)
10. X. Yang, P. Qiu, J. Yang, Y. Fan, L. Wang, W. Jiang, X. Cheng, Y. Deng, W. Luo, Small **17**(9), 1904022 (2019)
11. A. Yamaguchi, M. Saiga, D. Inaba, M. Aizawa, Y. Shibuya, T. Itoh, Anal. Sci. **37**, 49 (2021)
12. Y. Bai, H. Yang, W. Yang, Y. Li, C. Sun, Sens. Actuators B **124**, 179 (2007)
13. Z. Dai, J. Bao, X. Yang, H. Ju, Biosens. Bioelectron. **23**, 1070 (2008)
14. K. Wang, H. Yang, L. Zhu, J. Liao, T. Lu, W. Xing, S. Xing, Q. Lv, J. Mol. Catal. B **58**, 194 (2009)
15. G. Zhou, K.K. Fung, L.W. Wong, Y. Chen, R. Renneberg, S. Yang, Talanta **84**, 659 (2011)
16. H. Li, J. He, Y. Zhao, D. Wu, Y. Cai, Q. Wei, M. Yang, Electrochim. Acta **56**, 2960 (2011)
17. J. Li, X. Qin, Z. Yang, H. Qi, Q. Xu, G. Diao, Talanta **104**, 116 (2013)
18. X. Cao, Y. Sun, Y. Ye, Y. Li, X. Ge, Anal. Methods **6**, 1448 (2014)
19. A.Y. Khan, S.B. Noronha, R. Bandyopadhyaya, Adv. Power Technol. **27**, 85 (2016)
20. J. Sheng, L. Zhang, J. Lei, H. Lu, Anal. Chim. Acta **709**, 41 (2012)

21. T. Itoh, T. Shimomura, A. Hayashi, A. Yamaguchi, N. Teramae, M. Ono, T. Tsunoda, F. Mizukami, G.D. Stucky, T. Hanaoka, Analyst **139**, 4654 (2014)
22. H. Mizuguchi, K. Sasaki, H. Ichinose, S. Seino, J. Sakurai, M. Iiyama, T. Kijima, K. Tachibana, T. Nishida, T. Takayanagi, J. Shida, Bull. Chem. Soc. Jpn. **90**, 1211 (2017)
23. S. Tvorynska, J. Barek, B. Josypcuk, Sens. Actuators B **344**, 130252 (2021)
24. K. Hosokawa, M. Omata, K. Sato, M. Maeda, Lab Chip **6**, 236 (2006)
25. I.-J. Chen, E. Lindner, Anal. Chem. **81**, 9955 (2009)
26. B.T. Good, C.N. Bowman, R.H. Davis, J. Colloid Interface Sci. **305**, 239 (2007)
27. J.Y. Park, C.M. Hwang, S.H. Lee, S.-H. Lee, Lab Chip **7**, 1673 (2007)
28. J.Y. Park, S.K. Kim, D.H. Woo, E.-J. Lee, J.H. Kim, S.H. Lee, Stem Cells **27**, 2646 (2009)
29. Z.-R. Xu, C.-G. Yang, C.-H. Liu, Z. Zhou, J. Fang, J.-H. Wang, Talanta **80**, 1088 (2010)
30. B.R. Bruhn, T.B.H. Schroeder, S. Li, Y.N. Billeh, K.W. Wang, M. Mayer, PLoS ONE **9**, e91350 (2014)
31. V. Narayanamurthy, Z.E. Jeroish, K.S. Bhuvaneshwari, P. Bayat, R. Premkumar, F. Samsuri, M.M. Yusoff, RSC Adv. **10**, 11652 (2020)
32. D. Lantigua, M.A. Nguyen, X. Wu, S. Suvarnapathaki, S. Kwon, W. Gavin, G. Camci-Unal, Soft Mater. **16**, 9242 (2020)
33. A. Tobitani, S.B. Ross-Murphy, Macromolecules **30**, 4845 (1997)
34. L.-C. Sang, M.-O. Coppens, Phys. Chem. Chem. Phys. **13**, 6689 (2011)
35. W. Fu, A. Yamaguchi, H. Kaneda, N. Teramae, Chem. Commun. **7**, 853 (2008)
36. E. L. Cussler, Diffusion: Mass transfer in fluid systems, 2nd eds. (Cambridge University Press, 1997)
37. Y. Zhou, J. Li, Y. Zhang, D. Dong, E. Zhang, F. Ji, Z. Qin, J. Yang, F. Yao, J. Phys. Chem. B **121**, 800 (2017)
38. P.M. Diakowski, H.-B. Kraatz, Chem. Commun. **10**, 1189 (2009)
39. X. Yang, Z. Zhou, D. Xiao, M.M.F. Choi, Biosens. Bioelectron. **21**, 1613 (2006)
40. A. Ahmad, Md.S. Akhtar, V. Bhakuni, Biochemistry **40**, 1945 (2001)
41. Y. Sugimoto, Y. Kitazumi, O. Shirai, M. Yamamoto, K. Kano, J. Phys. Chem. B **120**, 3122 (2016)
42. Y.-S. Liu, Y.-H. Hu, Q.-C. Hao, X.-M. Zhang, Z.-C. Liu, J.-G. Li, J. Chem. Eng. Data **54**, 739 (2009)
43. D. Bruen, C. Delaney, L. Florea, D. Diamond, Sensors **17**, 1866 (2017)
44. H. Mizuguchi, D. Nishimori, T. Kuwabara, M. Takeuchi, M. Iiyama, T. Takayanagi, Anal. Chim. Acta **1102**, 46 (2002)

Springer Nature or its licensor (e.g. a society or other partner) holds exclusive rights to this article under a publishing agreement with the author(s) or other rightsholder(s); author self-archiving of the accepted manuscript version of this article is solely governed by the terms of such publishing agreement and applicable law.